Relating atmospheric N_2O concentration to N_2O emission strength in the U. S. Corn Belt

Congsheng Fu[1,2], Xuhui Lee[1,2], Timothy J. Griffis[3], Edward J. Dlugokencky[4], Arlyn E. Andrews[4]

[1]Yale-NUIST Center on Atmospheric Environment, Nanjing University of Information Science and Technology, Nanjing, Jiangsu, China
[2]School of Forestry and Environmental Studies, Yale University, New Haven, CT, USA
[3]Department of Soil, Water, and Climate, University of Minnesota, Saint Paul, MN, USA
[4]Global Monitoring Division, NOAA Earth System Research Laboratory, Boulder, Colorado, USA

Correspondence to: Xuhui Lee (xuhui.lee@yale.edu)

Abstract. Nitrous oxide (N_2O) has a high global warming potential and depletes stratospheric ozone. The U. S. Corn Belt plays an important role in the global anthropogenic N_2O budget. To date, studies on local surface N_2O emissions and the atmospheric N_2O budget have commonly used Lagrangian models. In the present study, we used an Eulerian model - Weather Research and Forecasting Chemistry (WRF-Chem) model to investigate the relationships between N_2O emissions in the Corn Belt and observed atmospheric N_2O mixing ratios. ~~Modeled hourly N_2O mixing ratios were combined with continuous atmospheric N_2O measurements at the KCMP tall tower in Minnesota to constrain agricultural N_2O emissions~~We derived a simple equation to relate the emission strengths to atmospheric N_2O mixing ratios, and used the equation and hourly atmospheric N_2O measurements at the KCMP tall tower in Minnesota to constrain agricultural N_2O emissions. The modeled spatial patterns of atmospheric N_2O were ~~validated~~ evaluated against discrete observations at multiple tall towers in the NOAA flask network. After optimization of the surface flux, the model reproduced reasonably well the hourly N_2O mixing ratios monitored at the KCMP tower. Agricultural N_2O emissions in the EDGAR42 database needed to be scaled up by 19.0 to 28.1 fold to represent the true emissions in the Corn Belt fo~~rrom~~r June 1-20, 2010 - a peak emission period. Optimized ~~total~~ mean N_2O emissions were 3.00-4.38, 1.52-2.08, 0.61-0.81 and 0.56-0.75 nmol m^{-2} s^{-1} fo~~rrom~~r June 1-20, August 1-20, October 1-20 and December 1-20, 2010, respectively. The simulated spatial patterns of atmospheric N_2O mixing ratios after optimization were in good agreement with the NOAA discrete observations during the strong emission peak in June. Such spatial patterns suggest~~illustrate~~ that the underestimate of emissions using IPCC (Inter-governmental Panel on Climate Change) inventory methodology ~~underestimate of emissions~~ is not dependent on tower measurement location.

1 Introduction

Nitrous oxide (N_2O) is an important greenhouse gas whose global warming potential is 265 times that of CO_2 over a 100-year time horizon, and is the 3rd largest contributor to the increase in radiative forcing since 1750, only after CO_2 and CH_4 (Hofmann et al., 2006). In addition, N_2O has the largest ozone depletion potential ~~(ODP) weighted emissions~~ of substances that deplete stratospheric ozone (Ravishankara et al., 2009). It is inert in the troposphere with a lifetime longer than one hundred years (Prather et al., 2012, 2015). Globally-averaged atmospheric N_2O has been increasing at a rate of 0.7 – 0.8 ppb yr^{-1} since late-1970s (Prinn et al., 2000; Hall et al., 2007; Saikawa et al., 2014).

The U.S Corn Belt is an intensively managed agricultural region, where a substantial amount of nitrogen, approximately 7.7 Tg, is added to cropland in forms of synthetic fertilizer and manure each year (Griffis et al., 2013). The Corn Belt plays an important role in global anthropogenic N_2O emissions (Miller et al., 2012). Cropland N_2O emissions ~~is~~ are difficult to measure

due to the episodic nature of the emissions and the high spatial variability (Wagner-Riddle et al., 2007; Groffman et al., 2009), and Corn Belt N_2O emissions ~~is~~ are no exception.

Bottom-up and top-down methods are used to quantify N_2O emissions from the Corn Belt (Griffis et al., 2013; Zhang et al., 2014; Chen et al., 2016) and other agricultural regions in previous studies (Corazza et al., 2011; Rees et al., 2013). The bottom-up method determines the total emissions by multiplying N input or other activity data with an emission factor for each pathway (De Klein et al., 2006). Top-down estimates of the emissions are usually determined from observed atmospheric N_2O mixing ratios, a transport model, and ~~empirical equations for~~ model optimization. Emissions inferred by the top-down method are generally larger than those by the bottom-up method for the Corn Belt. For example, Griffis et al. (2013) used three boundary layer budget methods and N_2O monitored on a tall tower in Minnesota during 2010 – 2011 to do a top-down analysis, and found that the N_2O emissions in the Corn Belt ~~was~~ were 3 to 9 times larger than bottom-up estimates, including estimates based on the IPCC inventory methodology and the EDGAR (Emission Database for Global Atmospheric Research) version 4.2 and GEIA (Global Emissions InitiAtive) databases. Kort et al. (2008) constrained the N_2O emissions over the central U. S. and southern Canada using an inverse modeling method, and reported that emissions in EDGAR version 32FT2000 and in GEIA are underestimated by about three fold for May – June, 2003. Similarly, the top-down analysis of Miller et al. (2012) concluded that N_2O emissions in EDGAR4 (version 4.0) should be scaled by factors of 6.1 and 10.1 for June, 2004 and June, 2008, respectively, for the central U. S. Most recently, Chen et al. (2016) estimated N_2O emissions from the Corn Belt using a Bayesian inversion technique, concluding that both direct emissions from agricultural soils and indirect emissions from leaching and runoff are underestimated in EDGAR42, with the latter needing to be adjusted upward by 2.4 to 5.1 fold.

In the inverse analyses cited above, different emission databases (e.g., EDGAR 32 FT2000 and GEIA in Kort et al., 2008; the Dynamic Land-Ecosystem Model – DLEM in Tian et al., 2010; EDGAR4, EDGAR 32 FT2000, GEIA, and DLEM in Miller et al., 2012 and Xiang et al., 2013; EDGAR42, GEIA, and IPCC in Griffis et al., 2013; EDGAR42 and Community Land Model in Chen et al., 2016) are used to provide the *a priori* estimate of surface emissions, and the meteorological fields are simulated using mesoscale models such as the Weather Research and Forecasting (WRF) model (Skamarock et al., 2008) or regional reanalysis (Miller et al., 2012). All top-down inverse modeling studies described here used ~~The transport of N_2O in the atmosphere is usually simulated with~~ the Stochastic Time Inverted Lagrangian Transport (STILT) Model (Gerbig et al., 2003) to simulate the transport of N_2O in the atmosphere. An advantage of using STILT to conduct the inverse modeling for N_2O is that it needs much less computational resources than full three-dimensional Eulerian models.

Because ~~Langrangian models~~ STILT ~~simulate~~ simulates the mixing ratio at one single point in space, it ~~they~~ cannot quantify how the surface N_2O emissions influence the spatial characteristics of atmospheric N_2O mixing ratios. This problem is avoided by using Eulerian models. To the best of our knowledge, no modeling studies have been published on the relationship between the spatial characteristics of surface emissions and the atmospheric N_2O mixing ratio ~~at the regional scale~~ for the Corn Belt. It is recognized that some of the parameterizations in STILT, such as the turbulent velocity variance and the Lagrangian timescale, need refinement to improve model performance (Pillai et al. 2012~~,~~). ~~and Eulerian modeling can inform these refinement efforts.~~ On the other hand, Eulerian models cannot distinguish the contribution of a specific source to the atmospheric concentration. Overall, both Lagrangian (e.g., STILT) and Eulerian (e.g., WRF-Chem) models have their advantages and disadvantages in inverse analysis, and comparing their results obtained for the same region can inform refinement efforts on these models.

The WRF model coupled with chemistry (WRF-Chem) has been used to simulate the flux and transport of CO_2 (Ahmadov et al., 2009; Pillai et al., 2012) and CH_4 (Beck et al., 2013), and other reactive gases. We are not aware of WRF-Chem applications to simulating the flux and transport of N_2O. In this study, we used WRF-Chem to investigate the spatial characteristics and influence of Corn Belt N_2O emissions on atmospheric N_2O. Specifically, we aimed to: (1) establish ~~empirical~~

relationships between the surface emission strength and the N$_2$O mixing ratio in the atmospheric boundary layer from multiple modeling experiments; (2) estimate the actual emissions as some multiple of the agricultural N$_2$O emissions in EDGAR42 whereby the multiplier was obtained from ~~via a simple inverse analysis whereby~~ these relationships ~~were used to force agreement between modeled and~~ and the ~~observed~~ atmospheric N$_2$O observed on a tall tower in Minnesota; ~~and~~ (3) investigate

5 the spatial patterns of the N$_2$O mixing ratio in the atmospheric boundary layer; and (4) analyze uncertainties in the inverse analysis.

  This work is complementary to a recent study completed by Chen et al. (2016). They used the Lagrangian-based STILT model to simulate N$_2$O transport, and conducted an inverse analysis using the Bayesian method. The present study used Eulerian-based WRF-Chem to model N$_2$O transport, and used a simple empirical equation to do the inverse analysis. The inverse analysis

10 in Chen et al. (2016) was based on N$_2$O measured at a single height on a tower in Minnesota, while the present study used N$_2$O measured at multiple heights on the same tower, and analyzed the influences of monitoring height on the inverse analysis results. Additionally, the modeled N$_2$O mixing ratio in the present study was compared with observations of N$_2$O made by NOAA using discrete air samples collected at multiple sites. To our best knowledge, this study appears to be the first one that uses WRF-Chem to do inverse analysis for N$_2$O, analyzes the influences of monitoring height on the inverse analysis results, and illustrates

15 the spatial characteristics of the influences of the Corn Belt on the atmospheric N$_2$O concentration. Deployment of measurements made at multiple heights in inverse analysis can reduce the uncertainty in modeling transport and diffusion in the atmospheric boundary layer and therefore should provide better estimates of the actual emission than if only one measurement height is used.

2 Materials and methods

2.1 Observation

20 One set of atmospheric N$_2$O data came from observations at the KCMP radio communication tall tower (44.69° N, 93.07° W) in Minnesota, near the northern border of the Corn Belt (Fig. 1). Air was drawn from heights of 32, 56, 100, and 185 m above the ground into a tunable diode laser analyzer (TGA100A, Campbell Scientific Inc., Logan, Utah, USA) for continuous detection of the N$_2$O mixing ratio. Measurement was made at a sampling frequency of 10 Hz and was averaged to hourly values. The analyzer response was calibrated with standards on the NOAA 2006A N$_2$O mole fraction scale (Hall et al., 2007), and the hourly

25 calibration precision was estimated to be 0.5 ppb. Details regarding the measurements of the N$_2$O mixing ratio were described in Griffis et al. (2010; 2013). Data of four periods at the KCMP tower were used in the present study, namely, 1st – 20th in June, August, October, and December in 2010, representing early summer, late summer, fall and winter, respectively. The month of June 2010 had particularly large emissions (Griffis et al., 2013).

  The second dataset came from NOAA. Discrete air samples from six NOAA tall tower sites were collected daily during

30 18:00 – 21:00 (UTC) at heights of 107 – 457 m above the ground. The six sites are WBI (West Branch, Iowa), LEF (Park Falls, Wisconsin), SCT (Beech Island, South Carolina), BAO (Boulder Atmospheric Observatory, Colorado), AMT (Argyle, Maine), and WKT (Moody, Texas; Fig. 1). N$_2$O dry-air mole fractions were determined by gas chromatography with election capture detection. The analytical system was calibrated with standards on the NOAA 2006A N$_2$O mole fraction scale. The average repeatability was ~0.4 ppb.

35 The third set of data is hourly N$_2$O mixing ratio monitored at Niwot Ridge (NWR), Colorado (40.04° N, 105.54° W; elevation: 3018 m), which was used as background in the present study. The analyzer response was also calibrated with standards on the NOAA 2006A N$_2$O mole fraction scale. The reproducibility of N$_2$O calibrations in the ambient range was 0.22 ppb.

2.2 Model setup

The latest version of the WRF-Chem model (version 3.7.1) was used to simulate the meteorological field, and the transport and mixing of N_2O. In the model domain, N_2O was treated as a passive tracer. Fig. 1 shows the map of the Corn Belt, the locations of N_2O mixing ratio measurements, the modeling domains used in the present study, and ~~the total~~a ~~default~~ _prior_ emission flux density according to EDGAR42 plus EDGAR2 natural soil emissions. To represent the tall tower observations, atmospheric transport models should be configured with high spatial resolutions of 2 – 20 km (Phillai et al., 2012). In the modeling study of Miller et al. (2012), the outer and inner domains have a spatial resolution of 40 km and 10 km, respectively. In the present study, we deployed two nested domains. The outer domain had 44 × 34189 grids with a resolution of 70 km, and the inner domain had 34189 × 98 grids with a resolution of 10 km. Both domains had 40 vertical levels varying from the land surface to a pressure height of 50 hPa or approximately 20 km above the sea level. The meteorology module and chemistry module use the same mesh generation. The heights of layers 1, 2, and 3 are around 30, 100, and 190 m above the local terrain surface, respectively, so we compared the modeling results of these layers with observations at the height of 32, 100, and 185 m, respectively.

Because three-dimensional modeling of the meteorological field and the tracer transport requires substantial computational resources, it is not feasible to do the simulation continuously for a long period (e.g., one year). Instead, the model calculation was performed for four select periods (1st – 20th in June, August, October, and December in 2010). The initial and boundary conditions for the meteorological field were obtained from the weather forecast model Global Forecast System (ftp://nomads.ncdc.noaa.gov/GFS/analysis_only). The initial and boundary conditions for the N_2O mixing ratio for each modeling period were obtained from Model for Ozone and Related Chemical Tracers (MOZART) version 4 (http://www.acom.ucar.edu/wrf-chem/mozart.shtml). Cloud microphysics was represented with the single-moment 5-class scheme (WSM), the boundary layer was modeled with the Yonsei University Scheme (YSU), and the land surface was modeled with the Community Land Model Version 4 (CLM4). Other model settings are shown in Table 1.

The lower boundary condition for N_2O was a predetermined surface emission flux, which was constant in time but varied spatially. Both the EDGAR and the GEIA databases have surface emission data for the Corn Belt, and both have more detailed and reasonable spatial distributions than DLEM (Miller et al., 2012)~~. ; Because~~In comparison, EDGAR needs less magnitude correction than GEIA in inverse modeling (Miller et al., 2012; Griffis et al., 2013), so we used ~~the latest version of~~ EDGAR ~~(version 4.2)~~ as the default flux boundary condition. EDGAR42 N_2O emission data has a spatial resolution of 0.1° × 0.1°, close to the resolution of our inner model domain. The total EDGAR42 N_2O emissions (annual mean flux density) for the outer domain ~~is~~are 0.083 nmol m^{-2} s^{-1}, and corresponding value for the Corn Belt ~~is~~are 0.21 nmol m^{-2} s^{-1}. Agricultural sources of N_2O include manure management, agricultural soil, indirect emissions from agriculture, and agricultural biomass burning. The total agricultural emissions ~~rate is~~are 0.15 nmol m^{-2} s^{-1} for the Corn Belt (Supplementary Figure S1). The natural soil emission ~~rate~~s are 0.036 and 0.038 nmol m^{-2} s^{-1} for the outer domain and the Corn Belt, respectively. The spatial distribution of the sum of the EDGAR42 ~~flux~~ and natural soil emissions is shown in Fig. 1.

2.3 Experimental design

Because N_2O is inert in the troposphere, changes in its mixing ratio C are primarily controlled by variations in the surface source strength F and atmospheric transport. However, the relationship between C and F is not a 1:1 correspondence. Because of influences of wind direction and turbulent~~vertical~~ diffusion and convection, we do not expect the C enhancement in the atmospheric boundary layer to double in response to a doubling of F in the Corn Belt. Here we established the relationship between C and F using results of multiple model runs. Three different modeling experiments were conducted for each of the four study periods. The first run was a background simulation using the natural soil emissions and EDGAR42 non-agricultural

emissions for both domains. The resulting N$_2$O mixing ratio is taken as the background, C_b. The second model run was a default simulation driven by natural soil emissions and the total EDGAR42 emissions (agricultural and non-agricultural) in both domains. The third run was a scaled simulation whereby the surface flux in the grid cells belonging to the Corn Belt in the inner domain was the sum of natural soil emissions, EDGAR42 non-agricultural emissions, and a multiple of EDGAR42 agricultural emissions. The multiplier values are 3, 6, 12, and 25, the exact choice depending on the modeling period (Table 2). For the grid cells not belonging to the Corn Belt in the inner domain and the grid cells in the outer domain, the multiplier values are set to one. In the EDGAR inventory, the N$_2$O emission is determined with the IPCC-type methodology using agricultural activity data and standardized emission factors. Our study makes two implicit assumptions (1) that these emission factors are biased similarly in all model grids in the Corn Belt; and (2) that the observed concentration is equally sensitive to emissions everywhere in the Corn Belt.

The preset multipliers in Table 2 represent our first guess values. The actual multiplier values are constrained by the concentration observations at the KCMP tower. First, wWe define the concentration enhancement, ΔC, for the grid cell containing KCMP tower as the difference in N$_2$O mole fraction between the default or scaled simulation and the background simulation. Let concentration multiplier M_C be the ratio of ΔC from the scaled simulation to that from the default simulation and M_F be the emission flux multiplier. The two multipliers are related to one another as

$$M_C - 1 = a\,(M_F - 1) \tag{1}$$

where the empirical coefficient a (< 1) was determined with a least squares procedure from the modeled concentration data. The scaled simulations with multipliers of 3, 6, 12, and 25 are used to find parameter a in Equation (1).

Next, 2.4 A simple inverse analysis

wWe used the observed enhancement, ΔC, defined as the actual concentration observed at the KCMP tall tower minus a background concentration and adjusted for a small spatial gradient in the modeled N$_2$O mixing ratio between KCMP and the background concentration site from the background simulation, to constrain the flux multiplier (and the surface emission flux). A numerical example is given in the Supplementary Information on how this is done. The background concentration was observed at NWR, which is upwind of and outside the Corn Belt (Supplementary Table S1). The background value was calculated as a 3-day running mean. Another advantage of using NWR as opposed other NOAA monitoring sites is that the observation at NWR is continuous in time whereas measurements at other sites are made only once or twice per day. Griffis et al. (2013) and Chen et al. (2016) also used the observation at NWR as the background concentration.

If the EDGAR42 emission flux is accurate and the model is perfect, the observed ΔC should match with the concentration enhancement from the default model simulation. Any disagreement is caused either by model errors or by errors in the surface flux. Here we assume that the flux errors are solely responsible for the disagreement, leaving the discussion of model errors to a later part of the paper. Not surprisingly, the ΔC from the default simulation is always lower than the observed ΔC, meaning that the EDGAR42 emission flux is biased low. To find a correction factor, we should ideally run the WRF-Chem in an iterative fashion, by adjusting the surface flux repeatedly until the modeled ΔC matches the observed ΔC. However, this procedure is computationally prohibitive. Instead, we resorted to a simple two-step method. First, the concentration multiplier M_C was determined by dividing the mean observed ΔC with the mean modeled ΔC from the default simulation for each modeling period. Second, the M_C value was used in Equation (1) to find the emission multiplier M_F. The EDGAR42 agricultural emission flux times M_F is then regarded as the true agricultural flux.

An implicit assumption in this simple inverse analysis is that $M_C$$\Delta C$ should respond linearly to changes in the $M_F$surface flux. The Because N$_2$O is an inert gas, following results illustrate that this assumption is generally satisfied (see Fig. 2 3 below).

5

3 Results

In this section, we first compare the modeled mixing height with those derived from other data products to evaluate the accuracy of the modeled N_2O transport in the atmosphere. We then discuss the relationship between the modeled concentration enhancement and the flux enhancement; these results are used to establish Equation (1). The constrained emission flux values are given next. After that, we compare the modeled mixing ratio with the hourly observations at the KCMP tower and the modeled mixing ratio spatial distribution with those observed at multiple NOAA flask sites. Finally, we present the spatial distribution of the modeled atmospheric N_2O mixing ratio in the Corn Belt.

3.1 Mixing height

A key factor in inverse analysis is the accuracy of the modeled atmospheric N_2O transport and turbulent mixing. One source of model error stems from the vertical transport calculation. Previous studies have shown that the parameterizations of the PBL in WRF-Chem affects modeled scalar concentrations in the atmospheric boundary layer (Kretschmer et al., 2012). If vertical mixing is too strong, the emitted N_2O will spread over a deeper boundary layer, potentially causing a low bias in the modeled ΔC near the surface. The YSU scheme adopted in this study has been used successfully in previous WRF simulations (e.g., Pillai et al., 2012). Accuracy assessment results from Pillai et al. (2012) indicate that WRF-Chem using the YSU scheme can capture the hourly fluctuations of passive tracers at different heights near the ground.

The sensitivity to the diffusion scheme is manifested in the predicted mixed layer height z_i because a high bias in z_i will lead to a low bias in ΔC and vice versa. In an inverse modeling analysis of carbon monoxide, Kim et al. (2013) presented the diurnal cycle of z_i from four different meteorological simulations for the KCMP tower site, namely, EDAS (Eta Data Assimilation System), NARR (North American Regional Reanalysis) from the National Centers for Environmental Prediction (NCEP), BRAMS (Brazilian developments on the Regional Atmospheric Modeling System), and GEOS-5 (Goddard Earth Observing System Model, version 5). Their inverse analysis yields surface carbon monoxide emission estimates with reasonable accuracy, achieving an R^2 value of 0.48 between the measured and the simulated CO mixing ratios. Fig. 2 compares our modeled z_i diurnal cycle with those derived for 2009 from the three meteorological simulations (EDAS, NARR, and GEOS-5) in Kim et al. (2013) and with the 3-hourly NCEP-NARR data for the four exact 20-day periods in 2010 (Supplementary Figure S2). In this comparison, we omitted the BRAMS data because its z_i value is unreasonably high (Kim et al., 2013). Our modeled mean diurnal cycles of the mixing height during $1^{st} - 20^{th}$ in June, August, and October are broadly consistent with the results of NARR and with those reported by Kim et al. (2013). Even though the results in Kim et al. (2013) are for complete seasons in 2009 and the results in the present study are for shorter periods in 2010, this is a valid comparison because our summer periods occurred at the beginning and the end of the season and our fall period was in the middle of the season. For December $1^{st} - 20^{th}$, our z_i value is biased high by ~ 400 m and shows smaller diurnal variations in comparison with NARR. For this reason, we are less confident about the inverse result for this time period than for the other three time periods.

3.1 2 Emission enhancement versus concentration enhancement at the KCMP site

Because the KCMP tower is close to the northern boundary of the Corn Belt (Fig. 1), south wind is expected to cause larger N_2O mixing ratio enhancement than north wind. In Fig. 2a3a-c, the modeled ΔC at the height of 185 m from the scaled simulation with a flux multiplier M_F of 25 is plotted against the modeled ΔC from the default simulation for the time period from June 1 to 20, 2010. Each data point represents one hourly value. The data are sorted into three wind direction groups (90° – 270°, 270° – 90°, and 0° – 360°). Of the three wind groups, south wind with direction of 90° – 270° resulted in the largest N_2O mixing ratio

enhancement (Fig. ~~2b~~3b). The regression slope for this wind direction range is 18.66. In other words, at the flux multiplier M_F of 25, the concentration enhancement multiplier M_C is 18.66. The concentration multiplier is 11.47 for north wind (wind direction range 270° – 90°; Fig ~~2c~~3c) and is 15.71 if all wind directions are considered (Fig. ~~2a~~3a).

Similar analysis was applied to the other three modeling periods, each yielding a M_C value for each wind sector at the set M_F value given in Table 2. When the M_C versus M_F data pairs are put together for all four periods, a clear linear relationship is evident (Fig. ~~2d~~3d-f). Equation (1) with a coefficient value a of 0.740 best describes this relationship for south winds according to the least squares regression. The coefficient value is 0.470 for north winds and 0.631 for all wind directions. The value a of 0.740 for south winds is used for the inverse analysis presented below, because the observed N$_2$O mixing ratio could reasonably reflect emissions from the Corn Belt only during southerly winds.

3.~~2~~ 3 Constrained agricultural emission~~s~~

Because the KCMP site is close to the northern boundary of the Corn Belt, ~~the observed N₂O mixing ratio could reasonably reflect emissions from the Corn Belt only during southerly winds. Therefore,~~ data obtained for southerly flow were used to constrain the surface emission. As explained in Section 2.~~4~~3, the concentration multiplier M_C was computed as the ratio of the mean ΔC observed in south wind at the 185 m height to the mean ΔC from the default model simulation at the same height and also in south wind conditions. This M_C value was then used in Equation (1) with a = 0.740 to find the flux multiplier M_F. For example, for June 1-20, the concentration multiplier is 21.0, and the optimized flux multiplier is 28.1. A numerical example is given in the online Supplementary Information that outlines all the steps involved in this calculation.

Table 2 shows the constrained N$_2$O emission~~s~~ from the Corn Belt using the N$_2$O mixing ratio monitored at the height of 185 m on the KCMP tower. The constrained agricultural N$_2$O emissions for the 1st – 20th in June, August, October, and December are 4.29, 1.99, 0.72, and 0.66 nmol m^{-2} s^{-1}, respectively.

3.~~3~~ 4 Comparison of observed and adjusted model N$_2$O concentration

Fig. ~~3~~4 shows the observed (grey line), modeled (red line), and the adjusted model (blue line) N$_2$O mixing ratio enhancement at 185 m on the KCMP tower. The modeled and adjusted ΔC here is the concentration difference between the KCMP site and the NWR site. The modeled ΔC using a *prior* (default) emissions is the enhancement from the default simulation ~~and~~ plus a small concentration difference between the KCMP site and the NWR site from the background simulation, and the adjusted model ΔC is the enhancement from the default simulation~~default ΔC~~ times the appropriate concentration multiplier plus the concentration difference between the KCMP site and the NWR site from the background simulation. The modeled ΔC using ~~the~~ a ~~default~~ *prior* emission~~s~~ is clearly smaller than observation for all four periods (Fig. ~~3~~4). For example, for the model period June 1-20, the default model ΔC value is ~~0.18~~0.26 and ~~0.19~~0.35 ppb for all wind directions and for south wind, respectively, whereas the observed mean ΔC is 4.95 and 5.44 ppb, respectively. The south wind results yield a concentration multiplier of 28.1. After the adjustment, the modeled mixing ratio enhancements are much closer to the observations than those from the default simulation. The adjusted model ΔC can roughly reproduce the temporal fluctuations of the observed ΔC at the KCMP site, although the substantial noises, characterized by ~~(~~abrupt increases and decreases~~)~~ in the observation, result in low correlation coefficients between the simulated and the observed time series.

As shown in Fig. ~~2a~~3a-c, wind direction clearly affects the simulated ΔC. For the four study periods, the mean simulated ΔC under north wind conditions was roughly half of that under south wind conditions. The wind direction influence is also

evident in the hourly time variations of ΔC. For example, southern wind (wind direction 90° – 270°) prevailed during the four-day period from day of year 280 to 284, and the mixing ratio showed a gradual increasing trend with time.

Another factor that drives the temporal fluctuations of ΔC is the diurnal change of vertical mixing which is stronger in the day than at night. The larger daytime vertical diffusivity corresponds to the smaller modeled N_2O mixing ratio enhancement near the land surface. The intensity of vertical mixing can be reflected by the mixed layer height. The linear correlation coefficient between the modeled mixed layer height and the hourly modeled N$_2$O mixing ratio enhancement from the default simulation~~ΔC~~ was -0.45 and -0.19 for the KCMP grid at heights of 32 m and 185 m in August, respectively. The corresponding correlation values were -0.53 and -0.35 in October, -0.35 and -0.12 in June, and -0.32, and -0.15 in December. All of these correlations are significant (confidence level $p < 0.01$).

Accurate assessment of the model performance in reproducing the atmospheric N$_2$O mixing ratio is difficult at hourly intervals because of large measurement noise~~s~~. Here we compare the observed daily mean values with the daily simulated mean values using the ~~default~~ prior emission~~s~~, and the adjusted results (Fig. ~~4~~5). Without the flux adjustments, the modeled daily mean ΔC is about~~round~~ one fifth of~~an order of magnitude smaller than~~ the observed value. After the adjustments, the model result is closer to the observation, with a linear regression slope of 0.~~76~~75, and R^2 also improved from 0.~~01~~02 before the adjustments to 0.~~31~~35. Here one single concentration multiplier M_C value obtained for south wind conditions (e.g., $M_C = 21.0$ for June 1 - 20) was used to make the concentration adjustment to all hourly model values for each period, regardless of actual wind direction, and the daily mean adjusted value was based on these hourly adjusted values. If the adjustments are made separately to southern winds and to northern winds using the two different regression equations (Figure 2e and 2f), the adjusted daily model mean ΔC is improved even further: the regression slope of the adjusted model ΔC against the observed ΔC is 0.~~94~~90 and the R^2 is 0.~~34~~32.

The improvement brought by the optimization to the correlation between the modeled and observed concentrations is similar to that reported by Kim et al. (2013) for CO measured at the same tower. Their optimization improved their R^2 from 0.29 to 0.48, with an improvement of 0.19. The improvement of R^2 for N$_2$O in the present study is 0.33 (from 0.02 to 0.35). The R^2 value reported by Xiang et al. (2013) between optimized simulation results and the observation for the atmospheric N$_2$O concentration in California is 0.29 – 0.33, and is similar to ours. The remaining variations, not explained by the model, may be caused by the model's inherent limitation in terms of simulating boundary layer transport processes and by errors in the spatial distribution of the prior emissions.

3.~~4~~5 Spatial variations of modeled N$_2$O concentration

Currently, there are only a few stations monitoring atmospheric N$_2$O concentration in or near the Corn Belt. Detailed information on the spatial distribution of N$_2$O can help experimentalists position their observational sites strategically. It also reveals the spatial extent of the influences of local emissions on the atmosphere. Fig. ~~5a~~6a illustrates the mean modeled ΔC during June 1 – 20 for the modeling area from the scaled simulation run with a flux multiplier of 25.0, and Fig. ~~5b~~6b shows similar results as Fig. ~~5a~~6a but only for UTC hours 19 and 20. In Fig. 6b, the modeled ΔC value is interpolated to the measurement height of each site. The experimental flux multiplier of 25.0 is reasonably close to the optimized flux multiplier of 28.1. The actual concentration values at the tower sites in Fig. 6b are shown in Table 3. According to Table 3 and Fig. 6b, the modeled ΔC with $M_F = 25.0$ agrees reasonably well with the observations at WBI, LEF, SCT, and BAO for June 1st – 20th. Both the observed and modeled ΔC are largest at WBI, which is close to the center of the Corn Belt, among the six NOAA-PFP sites. The next highest ΔC is found at LEF, although a high model bias is evident there. The modeled and observed mean ΔC of these four sites located in the model domain are 1.51 and 1.27 ppb, respectively.

For August, October, and December with much weaker emissions than in June, the agreement between the observed and modeled ΔC is not as good. The observed N$_2$O mixing ratio at WBI near the center of the Corn Belt is even smaller than that at the background during October 1-20, as indicated by the negative ΔC (Table 3), which is unreasonable and suggests large uncertainties in the concentration measurements. The largest disagreement occurred in the October period: the modeled mean ΔC with $M_F = 3.0$ is 0.81 ppb for the four sites in the model domain but the observed mean ΔC is actually 0.01 ppb.

By measuring spatial variations in atmospheric N$_2$O, an observational network consisting of multiple sites has the potential to help constrain inverse analysis using Eulerian tracer transport models, if the measurement reflects true natural variations and is unaffected by measurement uncertainties. Given the flask measurement uncertainties noted above, such N$_2$O inversion would be difficult for low emission periods. The large measurement uncertainties may have explained why Miller et al. (2012) limited their geostatistical inversion to an early summer period.

In Fig. 5a6a, the maximum mean enhancement is 5.92 ppb, found at 93.20°W and 42.12° N, which is near the center of the Corn Belt and 286 km south of the KCMP tower. The mean modeled ΔC for the whole Corn Belt is 4.15 ppb at the height of 185 m above the ground, illustrating a clear influence of the Corn Belt on atmospheric N$_2$O.

The mean modeled ΔC at the KCMP tower is 3.69 ppb, slightly lower than the observed value of 4.95 ppb. Two reasons may explain this low bias. The fFirst minor reason is that, the results shown in Fig. 5 6 were from the scaled simulation with an experimental flux multiplier of 25.0, and this multiplier is slightly smaller than the optimized flux multiplier M_F value of 28.1 determined in post-simulation analysis. Second, the flux multiplier was calibrated to match the modeled results to observations during southerly winds, instead of all-wind conditions.

The modeled ΔC distribution resembles a rectangle that surrounds the Corn Belt, with a narrow dimension in the south-north direction and a wide dimension in the east-west direction, implying a larger spatial gradient in the south-north direction than in the east-west direction.

4 Discussion

4.1 Model accuracy

A key factor in inverse analysis is modeling accuracy. One source of model error stems from the vertical diffusion calculation. Previous studies have shown that the scheme describing diffusion in WRF-Chem affects modeled scalar concentrations in the atmospheric boundary layer (Kretschmer et al., 2012). If diffusion is too strong, the emitted N$_2$O will spread over a deeper boundary layer, potentially causing a low bias in the modeled ΔC near the surface. The YSU diffusion scheme adopted in this study has been used successfully in previous WRF simulations (e.g., Pillai et al., 2012). Accuracy assessment results from Pillai et al. (2012) indicate that WRF-Chem using the YSU scheme can capture the hourly fluctuations of passive tracers at different heights near the ground.

The sensitivity to the diffusion scheme is manifested in the predicted mixed layer height z_i because a high bias in z_i will lead to a low bias in ΔC and vice versa. In an inverse modeling analysis of carbon monoxide, Kim et al. (2013) presented the diurnal cycle of z_i from four different meteorological simulations for the KCMP tower site, namely, EDAS (Eta Data Assimilation System), NARR (North American Regional Reanalysis) from the National Centers for Environmental Prediction (NCEP), BRAMS (Brazilian developments on the Regional Atmospheric Modeling System), and GEOS-5 (Goddard Earth Observing System Model, version 5). Their inverse analysis yields surface carbon monoxide emission estimates with reasonable accuracy, achieving an R value of 0.69 between the measured and simulated CO mixing ratios. Fig. 6 compares our modeled z_i diurnal cycle with those derived for 2009 from the three meteorological simulations (EDAS, NARR, and GEOS-5) in Kim et al.

4.2 1 Sensitivity to measurement height

The analysis presented above is based on observations from 185 m on the KCMP tower. The inverse analysis was also repeated with observations from the heights of 32 m and 100 m. The optimized flux multipliers are summarized in Table 2. It is interesting that the optimized flux multiplier or the constrained emission flux increases with the observational height. The constrained flux is lowest if KCMP data obtained at 32 m were used and largest for data at 185 m. Theoretically, the constrained emissions should be independent of mixing ratio observation height if the N$_2$O mixing ratio is perfectly simulated. To help explain the height dependence, we compared the observed and modeled vertical N$_2$O mixing ratio gradients between 32 m and 185 m (Supplementary Figure S3). Both observed and modeled gradients were close to zero during the majority of the daytime periods (11:00 - 18:00 local time), with the mean value of (concentration at 32 m minus that at 185 m) 0.03 (observation) and

0.25 ppb (model) during 11:00 - 18:00 for June 1-20, illustrating strong vertical mixing in daylight hours. Here the model result was based on the simulation with an experimental flux multiplier of 25.0. During this period, the nighttime (21:00 - 06:00) gradient is greater, with the mean value of 1.44 ppb according to the observation and 5.47 ppb according to the model simulation. A similar diurnal pattern of the N_2O concentration gradient is also reported by Zhang et al. (2014). In the present study, the difference in vertical gradient between simulation and observation during night (5.47 ppb versus 1.44 ppb) is much larger than that during daytime (0.25 ppb versus 0.03 ppb), and contributes the most to the height dependence of the constrained emission flux.

We suggest that the bias in the modeled mixing ratio gradient and the height dependence of the constrained emission flux are mainly consequences of different footprints between the monitoring heights. According to STILT modeling results, the footprint for the height of 100 m at KCMP covers most of the continental U. S., and that for 185 m is at the continental scale (Kim et al., 2013; Chen et al., 2016), both of which are larger than the Corn Belt itself. As shown by Kort et al. (2008) and Miller et al. (2012), emissions outside the Corn Belt are probably underestimated by EDGAR database too. In other words, the concentration enhancement observed at 100 and 185 m at KCMP had contributions from agricultural sources both within and outside the Corn Belt, although being closer to the observation tower, the latter should outweigh the former. But in our analysis, adjustment was made only to the sources within the Corn Belt. To compensate for the EDGAR bias outside the belt, a large flux multiplier is required to force agreement between the modeled concentration and the observation at 100 or 185 m. Evidently, at nighttime when vertical mixing is weak, this large flux adjustment causes the modeled concentration at 32 m to increase more than that at 185 m, resulting in a high bias in the modeled concentration gradient. In this regard, the emission flux constrained with the data obtained at 32 m reflects more local sources than those constrained with the data obtained at higher levels, and may be a more accurate estimate of the emissions in the Corn Belt, considering that the landscapes around the KCMP tower are representative of the entire Corn Belt (Griffis et al., 2013). In view of this height dependence, the true flux mostly likely lies in the range of the optimized flux values based on measurements at these heights.

4.3 2 Comparison with other emissions estimates

According to our inverse analysis, agricultural N_2O emissions in the Corn Belt are 19.0 to 28.1 times the default EDGAR42 agricultural emissions during June 1 – 20, 2010, corresponding to an actual emission flux density of 2.91 – 4.29 nmol m^{-2} s^{-1}, with the upper and lower bounds determined by the concentration observed at 185 and 32 m, respectively. The total emissions, including agricultural, natural soil and non-agricultural sources is are 3.00 – 4.38 nmol m^{-2} s^{-1}. Using a nocturnal boundary layer method, Griffis et al. (2013) estimated that the Corn Belt emissions flux is are ~2.0 – 2.5 nmol m^{-2} s^{-1} in June and July 2010, which is ~0.5 – 1.0 nmol m^{-2} s^{-1} smaller than the lower bound of this study. From the results presented in Kort et al. (2008), we infer that their constrained N_2O emissions is are about 0.56 nmol m^{-2} s^{-1} in May – June, 2003 for the Corn Belt. Miller et al. (2012) reported that maximum emissions occurred in June in both 2004 and 2008, and their constrained emissions in June, 2008 is are approximately 1.20 nmol m^{-2} s^{-1} for the Corn Belt.

The differences between the present study and the previous studies are partly caused by the different spatial scales involved. In both the studies by Kort et al. (2008) and Miller et al. (2012), a single the emission scaling is applied to the entire modeling region (the continental U. S. and southern Canada in Kort et al., 2008; the central U. S. in Miller et al., 2012), instead of scaling the emissions for the Corn Belt only as in the present study. If they scaled the emissions for the Corn Belt only, the resulting emission flux would have probably been larger.

The annual N_2O emission flux from Corn Belt calculated using the IPCC inventory methodology is 0.19 nmol m^{-2} s^{-1} (Griffis et al., 2013), slightly smaller than the annual flux from Corn Belt in EDGAR42 – 0.21 nmol m^{-2} s^{-1}. The constrained annual N_2O emission flux over the central U. S. in Miller et al. (2012) is around 0.40 nmol m^{-2} s^{-1}, namely, around two times that from the IPCC inventory methodology. The constrained N_2O emission fluxes during the four study periods in the present study are all larger than those for the same periods in Miller et al. (2012), so the constrained N_2O emission fluxes from the Corn Belt are clearly larger than the values in EDGAR42 and those calculated using the IPCC inventory methodology.

Different study duration, time of the year, and study year also contribute to the different constrained emissions between the present and the former studies. In the present study, the early summer study period (June 1-20, 2010) is short and is timed with highest emission events. If we average the early summer and late summer (August 1 – 20), the emission flux is reduced to 2.26 – 3.23 nmol m^{-2} s^{-1}. Additionally, Kort et al. (2008) studied 2003 and Miller et al. (2012) studied 2008. The differences in the emission flux can be a result of increasing emissions with time. Based on our ongoing study, the N fertilizer input to the Corn Belt has averaged 6.2 ± 0.9 Tg N per year, and the trend is about 0.08 Tg N per year increase.

Our simulation results illustrate that the emission strength decreases quickly after August (Table 3; Fig. 3̶4), and such seasonal changes in 2010 in the present study are consistent with the results for other years in former inverse studies. For example, a quick decrease of N_2O emission strength since August also occurred in 2008 (Miller et al., 2012) and in 2009 (Zhang et al., 2014).

Our study confirms that the emission database EDGRA42 significantly underestimates agricultural N_2O emissions in the Corn Belt. Although our simple inverse analysis cannot identify which agricultural emission categories suffer biases, two recent studies indicate that the underestimation occurs to the indirect emissions associated with runoff and leaching. Turner et al. (2015) measured N_2O emissions from headwater streams in the Corn Belt, and reported that the IPCC indirect emission factors for rivers are underestimated up to nine fold in southern Minnesota. Using the STILT model and a Bayesian inversion technique, Chen et al. (2016) reported that the indirect emission flux in the Corn Belt is 2.4 – 5.1 fold as large as that estimated by the IPCC inventory methodology. Complementary to former Lagrangian approaches, the Eulerian approach used here places a spatially explicit constraint on the underestimate problem, illustrating that the IPCC methodology underestimate is not dependent on tower measurement location, i.e. WBI and KCMP would yield similar conclusions.

4.3 Other sources of uncertainty

Errors in the inverse analysis can arise from uncertainties in the model simulations and in the observed concentration. A large source of modeling uncertainties is related to the uniform scaling factor applied to the agricultural emissions in all the grid cells in the Corn Belt. Since sources closer to the observation tower have a stronger influence on the observed concentration than those farther away, a uniform scaling may bring some uncertainty into the inverse analysis. Miller et al. (2012) reported that the spatial patterns of the N_2O fluxes from both geostatistical and Bayesian inversions are strongly similar to that of nitrogen fertilizer application rate. We have analyzed the agricultural emission strength and the fertilization data and presented the results as functions of distance from the KCMP tower in the south wind sector (90° – 270°; Supplementary Figure S4). The two quantities show strongly similar overall decreasing trends as the distance from the KCMP tower increases, thus confirming that the dominant driver of spatial variations in N_2O agricultural emission is N fertilizer use. Within the radius of about 500 km from the tower, the emission strength and the fertilizer application rate are approximately constant with distance, noting that 500 km is the distance from the KCMP tower to the south boundary of the Corn Belt. Because of the lack of sensitivity to distance within the Corn Belt, the uncertainty caused by the uniform scaling of the prior is probably not too large.

To further investigate the inverse uncertainty, we have done additional modeling simulations by applying the scaling to the agricultural emissions in the whole modeling domain (including both the inner and the outer domain), instead of the Corn Belt only. The results, summarized in Supplementary Table S2, show that changes to the optimized flux is less than 14%. We have also done simulations by using the spatial distribution of the N_2O emission that strictly follows the spatial distribution of the fertilization rate. The results illustrate that changes to the optimized flux is less than 10% (Supplementary Table S3).

Another uncertainty in the modeling and the subsequent inverse analysis is the model background. Unlike some other modeling studies (e.g., Kort et al. 2008), here we compare the modeled N_2O concentration enhancement, instead of the absolute concentration itself, with the observation. The concentration enhancement is calculated as the difference in the N_2O mole fraction between the default or scaled simulation and the background simulation. The main purpose of doing this is to limit the effect of air mass origin. This effect is further reduced by using the initial and boundary conditions produced by a global model (MOZART4, http://www.acom.ucar.edu/wrf-chem/mozart.shtml).

The observation background is also a source of inverse uncertainty. In the present study, we used NWR as the background site for reasons stated in Section 2.3. We have also used AMT located downwind of the simulation domain (Fig. 1) as the background site to investigate the uncertainty caused by the background mixing ratio. The N_2O mixing ratio is nearly the same between the two background sites during June and December, but the mixing ratio at AMT is 0.6 – 0.8 ppb lower than at NWR in August and October (Supplementary Figure S5). The relative change in the optimized flux is 7 – 8% and 0 – 3% in June and December, respectively, and is 20 – 25% and 32 – 38% in August and October, respectively (Supplementary Table S4).

Uncertainties also exist in the monitoring data obtained at the KCMP tower. The abrupt increases and decreases by as much as 31 ppb in less than 2 hours in the observed N_2O mixing ratio (e.g., at day of year 160 and 164, Fig. 3a) are clearly measurement noise related to the sampling and calibration procedures. Such large measurement noises may be one reason for why even after optimization, the correlation between the modeled and observed concentrations is not very strong.

5 Summary

In the present study, we investigated the relationships between the N_2O emissions from the Corn Belt and the atmospheric N_2O mixing ratio using the WRF-Chem model, derived simple empirical equations for relating changes in the atmospheric mixing ratio to changes in the surface emission flux, and used the hourly N_2O mixing ratio monitored at the KCMP tower to constrain the agricultural N_2O emissions. The key findings are summarized as follows:

- By treating N_2O as an inert tracer, the WRF-Chem model could simulate atmospheric N_2O at high temporal (hourly) and spatial (10 km) resolutions and with reasonable accuracy. Following surface flux optimization, the model explained 3135% (185 m) – 3538% (32 m) of the observed variations in the daily mean N_2O mixing ratio at KCMP.

- The EDGAR42 database underestimated agricultural N_2O emissions in the Corn Belt for all four model periods (1st to 20th in June, August, October and December, 2010). The largest bias occurred in June: a simple inverse analysis indicates that actual agricultural emissions were 19.0 to 28.1 times EDGAR42 emissions.

- According to our inverse analysis, the total mean emissions, including natural soil emissions and total EDGAR42 emissions (agricultural and non-agricultural), was were 3.00-4.38, 1.52-2.08, 0.61-0.81 and 0.56-0.75 nmol m^{-2} s^{-1} in June, August, October and December 2010, respectively. The lower and upper bounds of these ranges were determined with observations at 32 m and 185 m on the KCMP tower, respectively.

- The simulated spatial patterns of atmospheric N_2O mixing ratios are in good agreement with observations from discrete air samples made by the NOAA during June, which is a strong emission peak. In the other three modeling periods, the

modeled mixing ratio and the network observations show some disparity. The IPCC underestimate of agricultural N₂O emissions in the Corn Belt using IPCC inventory methodology is not dependent on tower measurement location.

References

Ahmadov, R., Gerbig, C., Kretschmer, R., Körner, S., Rödenbeck, C., Bousquet, P., and Ramonet, M.: Comparing high resolution WRF-VPRM simulations and two global CO_2 transport models with coastal tower measurements of CO_2, Biogeosciences, 6, 807-817, doi:10.5194/bg-6-807-2009, 2009.

Beck, V., Gerbig, C., Koch, T., Bela, M. M., Longo, K. M., Freitas, S. R., Kaplan, J. O., Prigent, C., Bergamaschi, P., and Heimann, M.: WRF-Chem simulations in the Amazon region during wet and dry season transitions: evaluation of methane models and wetland inundation maps, Atmos. Chem. Phys., 13, 7961-7982, doi:10.5194/acp-13-7961-2013, 2013.

Corazza, M., Bergamaschi, P., Vermeulen, A. T., Aalto, T., Haszpra, L., Meinhardt, F., O'Doherty, S., Thompson, R., Moncrieff, J., Popa, E., Steinbacher, M., Jordan, A., Dlugokencky, E., Brühl, C., Krol, M., and Dentener, F.: Inverse modelling of European N2O emissions: assimilating observations from different networks, Atmos. Chem. Phys., 11, 2381-2398, doi:10.5194/acp-11-2381-2011, 2011.

Chen, Z., Griffis, T. J., Millet, D. B., Wood, J., Lee, X., Baker, J. M., Xiao, K., Turner, P., Chen, M., and Zobitz, J.: Partitioning N₂O emissions within the US Corn Belt using an inverse modeling approach, 2016. Global Biogeochemical Cycles, 30,1192–1205, doi:10.1002/2015GB005313in press, 2016.

De Klein, C., Novoa, R. S. A., Ogle, S., Smith, K. A., Rochette, P., Wirth, T. C., McConkey, B. G., Mosier, A., and Rypdal, K.: N₂O emissions from managed soils, and CO_2 emissions from lime and urea application, in 2006 IPCC Guidelines for National Greenhouse Gas Inventories, Vol 4: Agriculture, Forestry and Other Land Use, edited by H. S. Eggleston et al., pp. 11.11–11.54, Institute for Global Environmental Strategies (IGES), Intergovernmental Panel on Climate Change (IPPC), Kanagawa, Japan, 2006.

Gerbig, C., Lin, J. C., Wofsy, S. C., Daube, B. C., Andrews, A. E., Stephens, B. B., Bakwin, P. S., and Grainger, C. A.: Toward constraining regional-scale fluxes of CO_2 with atmospheric observations over a continent: 2. Analysis of COBRA data using a receptor-oriented framework, J. Geophys. Res.-Atmos., 108, 4757, doi:10.1029/2003JD003770, 2003.

Griffis, T. J., Baker, J. M., Sargent, S. D., Erickson, M., Corcoran, J., Chen, M., and Billmark, K.: Influence of C₄ vegetation on ¹³CO_2 discrimination and isoforcing in the upper Midwest, United States, Global Biogeochem. Cycles, 24, GB4006, doi:10.1029/2009GB003768, 2010.

Griffis, T. J., Lee, X., Baker, J. M., Russelle, M. P., Zhang, X., Venterea, R., and Millet, D. B.: Reconciling the differences

between top-down and bottom-up estimates of nitrous oxide emissions for the U.S. Corn Belt, Global Biogeochem. Cycles, 27, 746–754, doi:10.1002/gbc.20066, 2013.

Groffman, P. M., Butterbach-Bahl, K., Fulweiler, R. W., Gold, A. J., Morse, J. L., Stander, E. K., Tague, C., Tonitto, C., and Vidon, P.: Challenges to incorporating spatially and temporally explicit phenomena (hotspots and hot moments) in denitrification models, Biogeochemistry, 93(1-2), 49–77, doi: 10.1007/s10533-008-9277-5, 2009.

Hall, B. D., Dutton, G. S., and Elkins, J. W.: The NOAA nitrous oxide standard scale for atmospheric observations, J. Geophys. Res., 112, D09305, doi:10.1029/2006JD007954, 2007.

Hofmann, D. J., Butler, J. H., Dlugokencky, E. J., Elkins, J. W., Masarie, K., Montzka, S. A., and Tans, P.: The role of carbon dioxide in climate forcing from 1979 – 2004: Introduction of the annual greenhouse gas index, Tellus, Ser. B, 58, 614–619, doi: 10.1111/j.1600-0889.2006.00201.x, 2006.

Kim, S. Y., Millet, D. B., Hu, L., Mohr, M. J., Griffis, T. J., Wen, D., Lin, J. C., Miller, S. M., and Longo, M.: Constraints on Carbon Monoxide Emissions Based on Tall Tower Measurements in the U.S. Upper Midwest, Environ. Sci. Technol., 47 (15), 8316–8324, do: 10.1021/es4009486, 2013.

Kort, E. A., Eluszkiewicz, J., Stephens, B. B., Miller, J. B., Gerbig, C., Nehrkorn, T., Daube, B. C., Kaplan, J. O., Houweling, S., and Wofsy, S. C.: Emissions of CH_4 and N_2O over the United States and Canada based on a receptor-oriented modeling framework and COBRA-NA atmospheric observations, Geophys. Res. Lett., 35, L18808, doi:10.1029/2008GL034031, 2008.

Kretschmer, R., Gerbig, C., Karstens, U., and Koch, F.-T.: Error characterization of CO_2 vertical mixing in the atmospheric transport model WRF-VPRM, Atmos. Chem. Phys., 12, 2441-2458, doi:10.5194/acp-12-2441-2012, 2012.

Miller, S. M., Kort, E. A., Hirsch, A. I., Dlugokencky, E. J., Andrews, A. E., Xu, X., Tian, H., Nehrkorn, T., Eluszkiewicz, J., Michalak, A. M., and Wofsy, S. C.: Regional sources of nitrous oxide over the United States: Seasonal variation and spatial distribution, J. Geophys. Res., 117, D06310, doi:10.1029/2011JD016951, 2012.

Pielke, R. A., Cotton, W. R., Walko, R. L., Tremback, C. J., Lyons, W. A., Grasso, L. D., Nicholls, M. E., Moran, M. D., Wesley, D. A., Lee, T. J., Copeland, J. H.: A comprehensive meteorological modeling system–RAMS, Meteorol. Atmos. Phys., 49(1–4), 69–91, 1992.

Pillai, D., Gerbig, C., Kretschmer, R., Beck, V., Karstens, U., Neininger, B., and Heimann, M.: Comparing Lagrangian and Eulerian models for CO_2 transport – a step towards Bayesian inverse modeling using WRF/STILT-VPRM, Atmos. Chem. Phys., 12, 8979-8991, doi:10.5194/acp-12-8979-2012, 2012.

Prather, M. J., Holmes, C. D., and Hsu, J.: Reactive greenhouse gas scenarios: Systematic exploration of uncertainties and the role of atmospheric chemistry, Geophys. Res. Lett., 39, L09803, doi:10.1029/2012GL051440, 2012.

Prather, M. J., Hsu, J., DeLuca, N. M., Jackman, C. H., Oman, L. D., Douglass, A. R., Fleming, E. L., Strahan, S. E., Steenrod, S. D., Søvde, O. A., Isaksen, I. S. A., Froidevaux, L., and Funke, B.: Measuring and modeling the lifetime of nitrous oxide including its variability, J. Geophys. Res. Atmos., 120, 5693–5705, doi:10.1002/2015JD023267, 2015.

Prinn, R. G., Weiss, R. F., Fraser, P. J., Simmonds, P. G., Cunnold, D. M., Alyea, F. N., O'Doherty, S., Salameh, P., Miller, B. R., Huang, J., Wang, R. H. J., Hartley, D. E., Harth, C., Steele, L. P., Sturrock, G., Midgley, P. M., McCulloch, A.: A history of chemically and radiatively important gases in air deduced from ALE/GAGE/AGAGE, J. Geophys. Res., 105, 17,751–17,792, doi: 10.1029/2000JD900141, 2000.

Ravishankara, A. R., Daniel, J. S., and Portmann, R. W.: Nitrous oxide: The dominant ozone-depleting substance emitted in the 21st century, Science, 326, 123–125, doi: 10.1126/science.1176985, 2009.

Rees, R. M., Augustin, J., Alberti, G., Ball, B. C., Boeckx, P., Cantarel, A., Castaldi, S., Chirinda, N., Chojnicki, B., Giebels, M.,

Gordon, H., Grosz, B., Horvath, L., Juszczak, R., Kasimir Klemedtsson, Å., Klemedtsson, L., Medinets, S., Machon, A., Mapanda, F., Nyamangara, J., Olesen, J. E., Reay, D. S., Sanchez, L., Sanz Cobena, A., Smith, K. A., Sowerby, A., Sommer, M., Soussana, J. F., Stenberg, M., Topp, C. F. E., van Cleemput, O., Vallejo, A., Watson, C. A., and Wuta, M.: Nitrous oxide emissions from European agriculture – an analysis of variability and drivers of emissions from field experiments, Biogeosciences, 10, 2671-2682, doi:10.5194/bg-10-2671-2013, 2013.

Saikawa, E., Prinn, R. G., Dlugokencky, E., Ishijima, K., Dutton, G. S., Hall, B. D., Langenfelds, R., Tohjima, Y., Machida, T., Manizza, M., Rigby, M., O'Doherty, S., Patra, P. K., Harth, C. M., Weiss, R. F., Krummel, P. B., van der Schoot, M., Fraser, P. J., Steele, L. P., Aoki, S., Nakazawa, T., and Elkins, J. W.: Global and regional emissions estimates for N2O, Atmos. Chem. Phys., 14, 4617-4641, doi:10.5194/acp-14-4617-2014, 2014.

Skamarock, W., Klemp, J., Dudhia, J., Gill, D., Barker, D., Duda, M., Huang, X., Wang, W., and Powers, J.: A description of the advanced research WRF version 3, NCAR/TN–475+STR, Natl. Cent. for Atmos. Res., Boulder, Colo, 2008.

Tian, H., Xu, X., Liu, M., Ren, W., Zhang, C., Chen, G., and Lu, C.: Spatial and temporal patterns of CH_4 and N_2O fluxes in terrestrial ecosystems of North America during 1979-2008: Application of a global biogeochemistry model, Biogeosciences, 7, 2673–2694, doi:10.5194/bg-7-2673-2010, 2010.

Turner, P. T., Griffis, T. J., Lee, X., Baker, J. M., Venterea, R. T., and Wood, J. D.: Indirect nitrous oxide emissions from streams within the US Corn Belt scale with stream order, Proc Natl Acad Sci U S A. 112(32), 9839–9843, doi:10.1073/pnas.1503598112, 2015.

USDA National Agricultural Statistics Service. Statistics of fertilizer and pesticides. Available at https://www.nass.usda.gov/Publications/Ag_Statistics/2011/Chapter14.pdf, USDA-NASS, Washington, DC, 2011.

Wagner-Riddle, C., Furon, A., Mclaughlin, N. L., Lee, I., Barbeau, J., Jayasundara, S., Parkin, G., Von Bertoldi, P., and Warland, J.: Intensive measurement of nitrous oxide emissions from a corn-soybeanwheat rotation under two contrasting management systems over 5 years, Global Change Biol., 13(8), 1722–1736, doi:10.1111/j.1365-2486.2007.01388.x, 2007.

Xiang, B., Miller, S. M., Kort, E. A., Santoni, G. W., Daube, B. C., Commane, R., Angevine, W. M., Ryerson, T. B., Trainer, M. K., Andrews, A. E., Nehrkorn, T., Tian, H., and Wofsy, S. C.: Nitrous oxide (N_2O) emissions from California based on 2010 CalNex airborne measurements, J. Geophys. Res. Atmos., 118, 2809–2820, doi:10.1002/jgrd.50189, 2013.

Zhang, X., Lee, X., Griffis, T. J., Baker, J. M., and Xiao, W.: Estimating regional greenhouse gas fluxes: an uncertainty analysis of planetary boundary layer techniques and bottom-up inventories, Atmos. Chem. Phys., 14, 10705-10719, doi:10.5194/acp-14-10705-2014, 2014.

Table 1. WRF- Chem model configuration.

Basic equations	Non-hydro mode
Time-integration scheme	Runge-Kutta 3rd order
Time step for integration	120 s
Microphysics	WRF Single-Moment (WSM) 5-class scheme
Longwave radiation	Rapid Radiative Transfer Model (RRTM)
Shortwave radiation	Goddard Shortwave scheme
Cumulus	Grell-Devenyi ensemble scheme
Boundary-layer	Yonsei University Scheme (YSU) scheme
Surface-layer	Monin-Obukhov Similarity scheme
Land-surface	Community Land Model Version 4 (CLM4)

5

10

15

20

25

30

35

40

Table 2. Experimental and optimized flux multiplier M_F. Values in brackets are constrained agricultural emission flux in units of nmol m^{-2} s^{-1}.

Time	June 1 – 20	August 1 – 20	October 1 – 20	December 1 – 20
Experimental	0, 1, 25	0, 1, 12	0, 1, 3	0, 1, 6
Optimized [a]	19.0 (2.91)	9.3 (1.43)	3.4 (0.52)	3.0 (0.47)
Optimized [b]	22.5 (3.44)	11.6 (1.77)	3.8 (0.59)	3.6 (0.55)
Optimized [c]	28.1 (4.29)	13.0 (1.99)	4.7 (0.72)	4.3 (0.66)

Notes: a, b, c: using observation data at heights of 32, 100, and 185 m, respectively.

5

10

15

20

25

30

35

40

Table 3. Modeled and observed N$_2$O mixing ratio enhancements (ppb) for 1900 and 2000 UTC from NOAA. Measurements from Niwot Ridge (NWR) were used as background to determine the enhancement.

Site ID		Within modeling domain					Outside modeling domain		
		WBI	LEF	SCT	BAO	Mean	AMT	WKT	Mean
Sample height (m)		378.9	396	304.8	300	ΔC	107	457.1	ΔC
June 1 – 20	Observation	3.28	0.80	0.79	0.22	1.27	0	0.46	0.23
	Model with M_F =1	0.14	0.17	0.28	0.14	0.18	–	–	–
	Model with M_F =25	3.67	1.26	0.90	0.20	1.51	–	–	–
August 1 – 20	Observation	0.69	-0.04	0.40	0.35	0.35	-0. 77	0.02	0.02
	Model with M_F = 1	0.44	0.13	0.36	0.12	0.26	–	–	–
	Model with M_F = 12	2.82	0.87	0.41	0.15	1.06	–	–	–
October 1 – 20	Observation	-0.03	-0.55	0.50	0.11	0.01	-0.79	-0.35	-0.57
	Model with M_F = 1	0.86	0.56	0.58	0.21	0.55	–	–	–
	Model with M_F = 3	1.52	0.85	0.66	0.22	0.81	–	–	–
December 1 – 20	Observation	0.99	0.43	1.26	0.61	0.82	0.49	0.79	0.64
	Model with M_F = 1	1.22	0.36	0.85	0.14	0.64	–	–	–
	Model with M_F = 6	2.98	0.55	1.25	0.15	1.23	–	–	–

Notes: AMT – Argyle, Maine, Central Daylight Time (CDT) = UTC – 4; BAO – Boulder Atmospheric Observatory, Colorado, CDT = UTC – 6; LEF – Park Falls, Wisconsin, CDT = UTC – 5; SCT – Beech Island, South Carolina, CDT = UTC – 4; WBI – West Branch, Iowa, CDT = UTC – 5; WKT – Moody, Texas, CDT = UTC – 5.
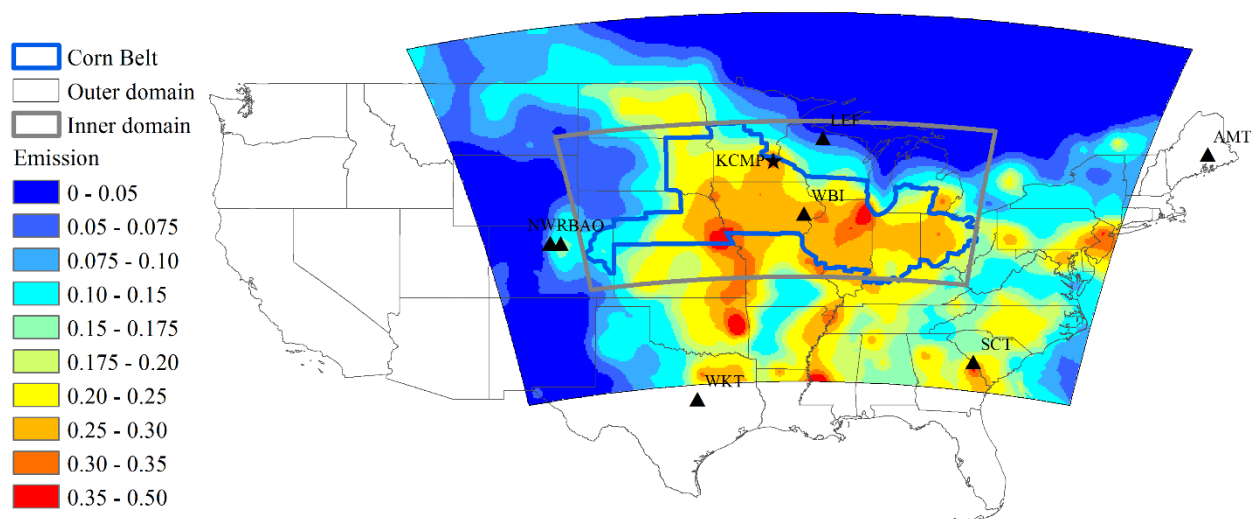
Figure 1. Locations of the N$_2$O monitoring sites, scope of the Corn Belt, modeling domains, and the prior~~default~~ N$_2$O emission flux in nmol m^{-2} s^{-1}. KCMP – Minnesota; NWR –Niwot Ridge, Colorado; AMT – Argyle, Maine; BAO – Boulder Atmospheric Observatory, Colorado; LEF – Park Falls, Wisconsin; SCT – Beech Island, South Carolina; WBI – West Branch, Iowa; WKT – Moody, Texas.
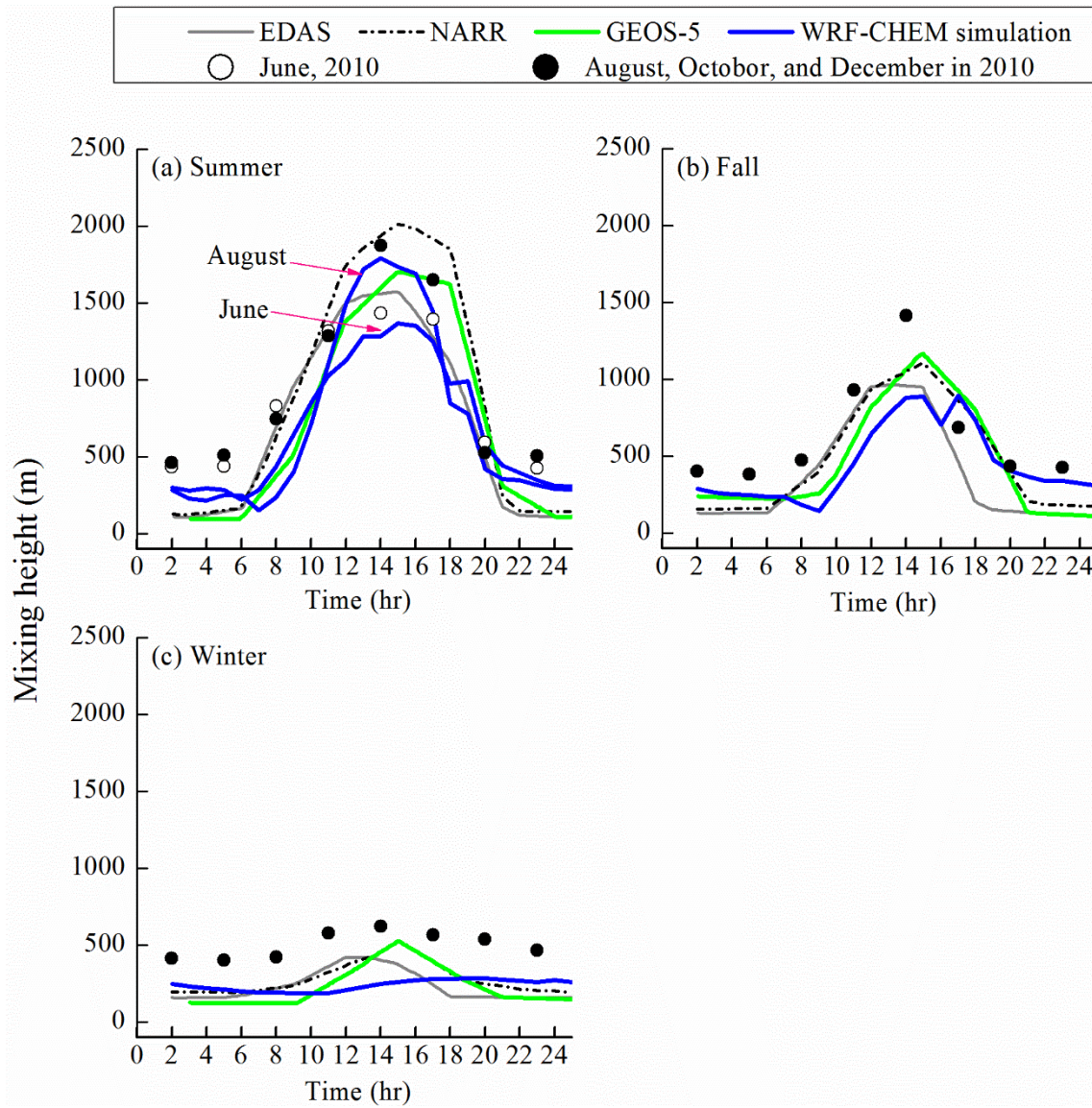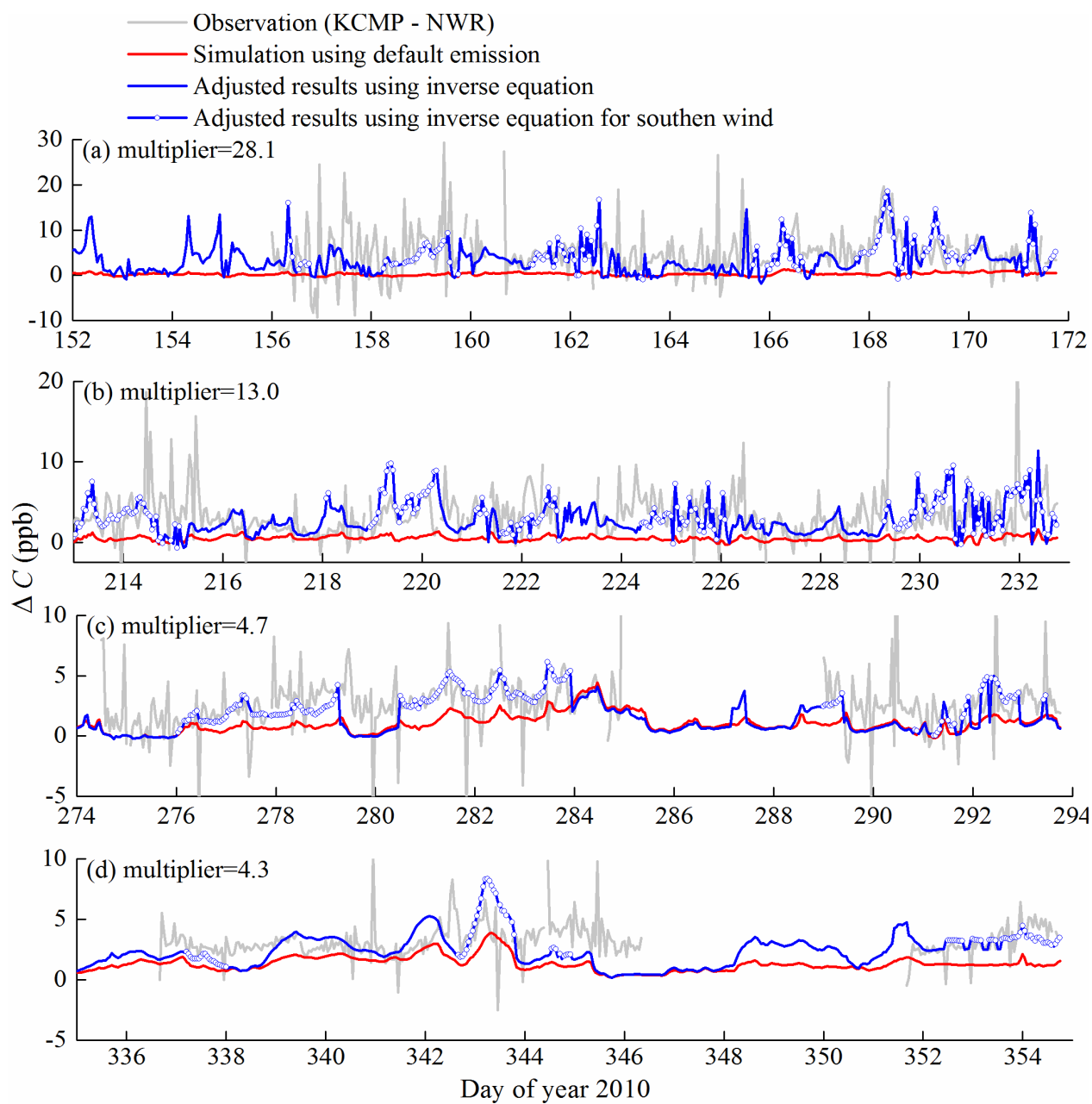
Figure 2. Simulated mixing height at the KCMP tower site in the present study (blue lines) and in Kim et al. (2013) (grey, black, and green lines) and the NCEP-NARR data (dots).
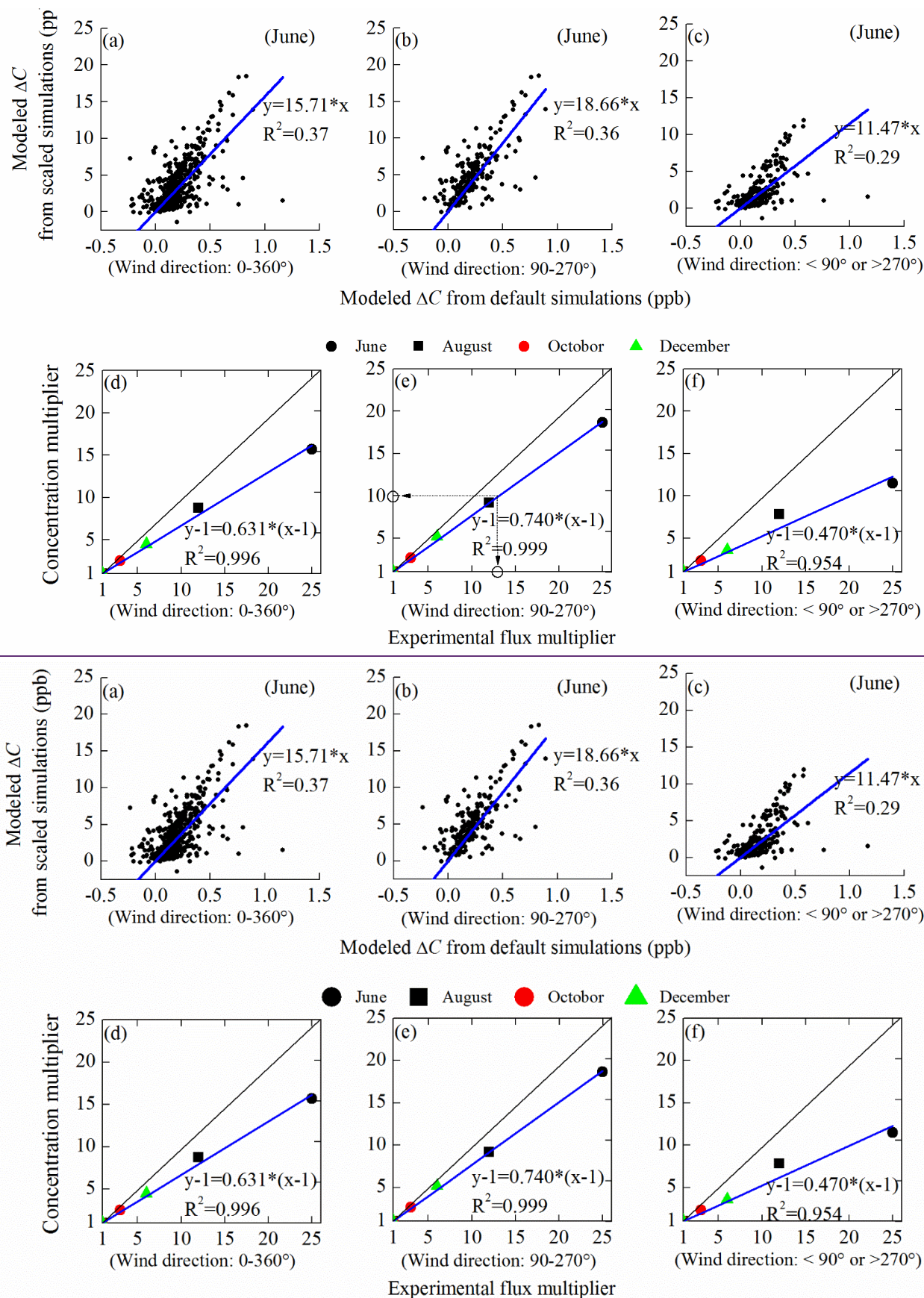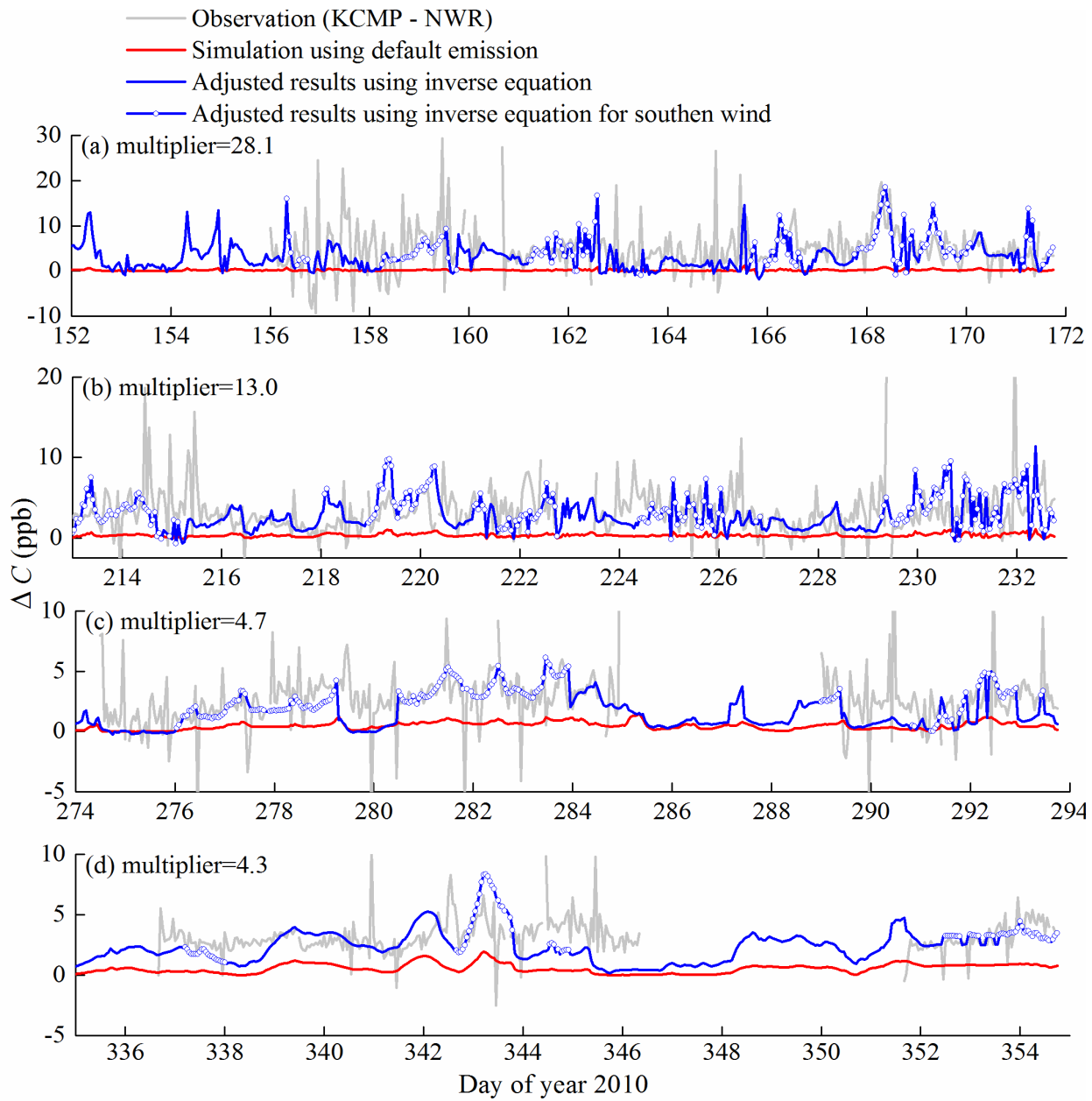
Figure 23. Relationships ~~of~~ for different model runs between concentration multiplier and experimental flux multiplier. The modeled N_2O mixing ratio enhancement ΔC was obtained from default and scaled simulations for 185 m at the KCMP tower. The scale simulation shown in panels a – c uses a multiplier of 25.0. The regression slope in panels a – c is represented by the

black circle in panels d – f. The hollow dots and dot lines in sub-figure (e) show how the emission flux multiplier M_F (the dot on x axis) is induced via the concentration multiplier M_C (the dot on y axis) for October 1-20.

Legend:
- Observation (KCMP - NWR)
- Simulation using default emission
- Adjusted results using inverse equation
- Adjusted results using inverse equation for southen wind

(a) multiplier=28.1

(b) multiplier=13.0

(c) multiplier=4.7

(d) multiplier=4.3

ΔC (ppb)

Day of year 2010

Figure 3̶4̲. Comparison of N$_2$O mixing ratio enhancement (ΔC) between observation (grey line), default model simulation (red line), and the scaled model simulation (blue line) for the height of 185 m at the KCMP tower site. Periods with south wind (wind direction: 90 – 270º) are marked by dots.

5
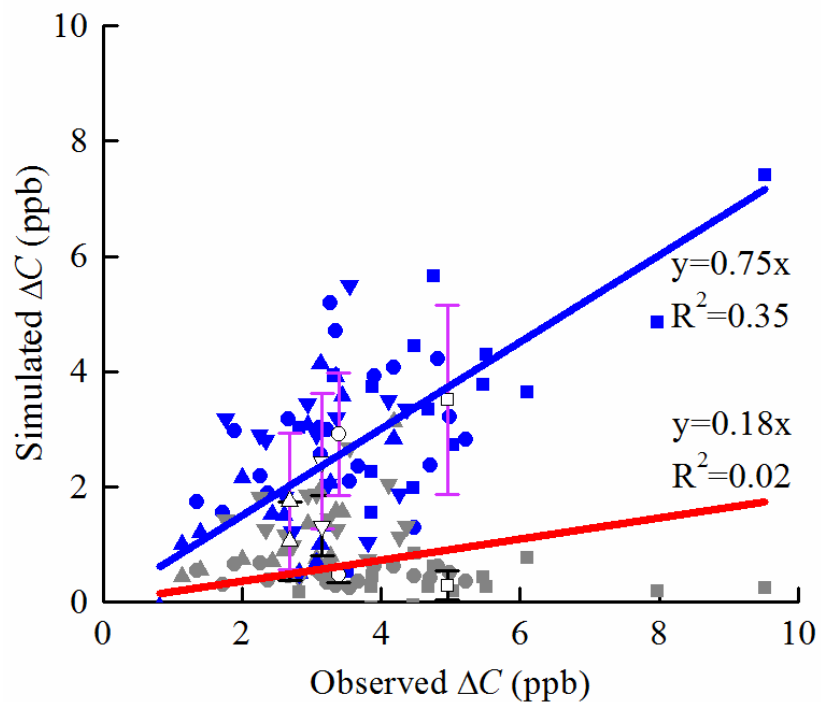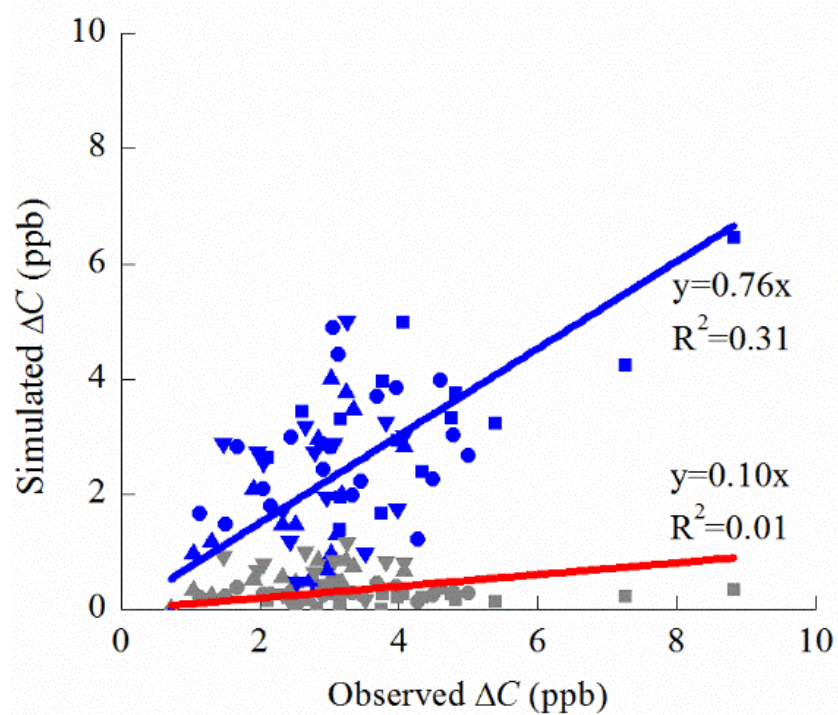
Figure 4~~4~~5. Correlations between the observed and scaled daily N$_2$O mixing ratio enhancement (ΔC) at the KCMP tower at 185 m.

(a) multiplier=25.0

(b) multiplier=25.0
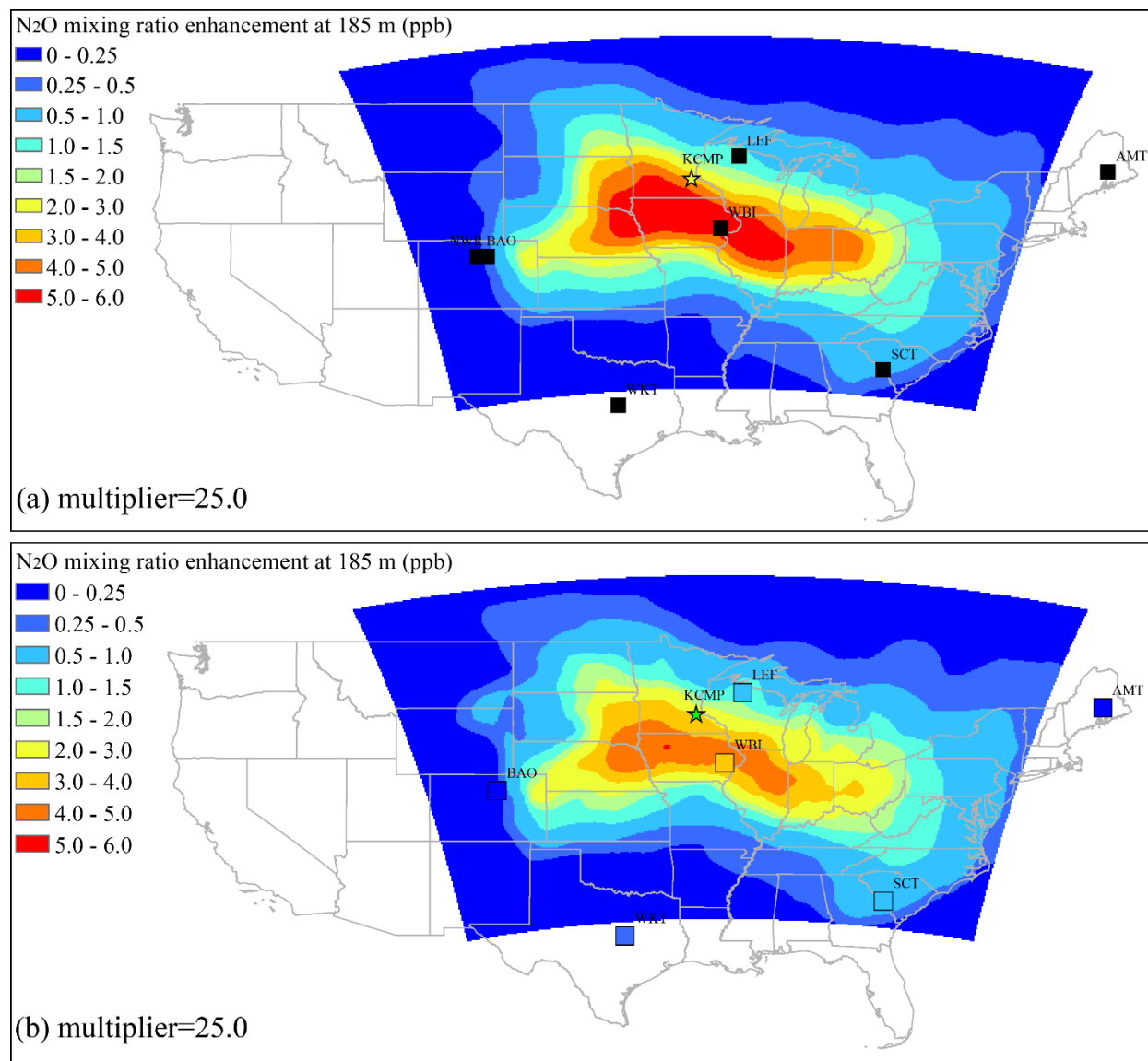
Figure ~~5~~6. Spatial characteristics of the mean modeled N$_2$O mixing ratio enhancement during June 1 – 20: (a) modeled results for all hours; (b) modeled results for UTC hours 19 and 20 only.
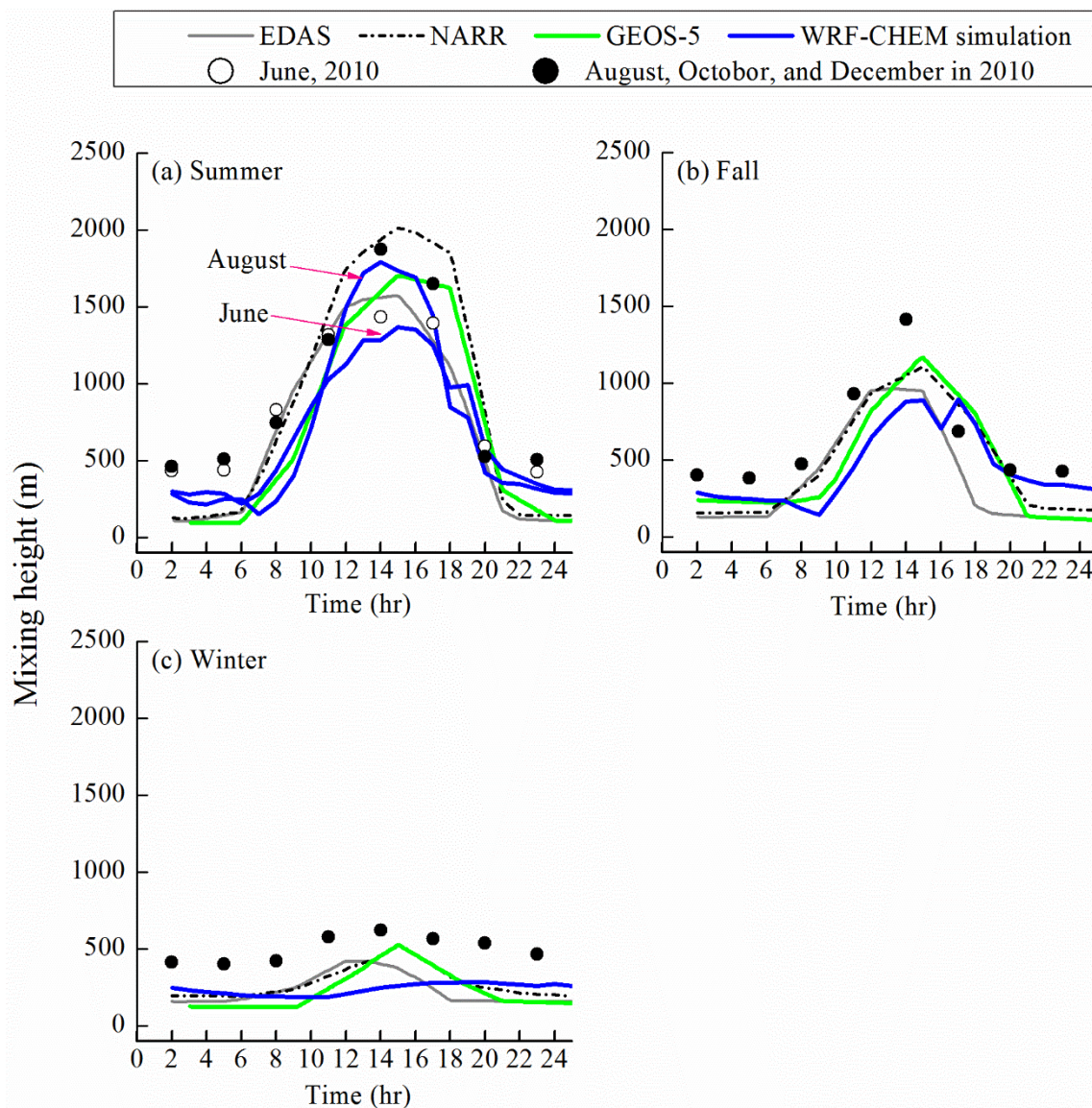
Figure 6. Simulated mixing height at the KCMP tower site in the present study (blue lines) and in Kim et al. (2013) (grey, black, and green lines) and the NCEP-NARR data (dots).